Pergamon

Journal of Structural Geology, Vol. 19, No. 11, pp. 1393 to 1404, 1997

0191-8141/97 $17.00 + 0.00

PII: S0191-8141(97)00057-6

Permeability of fault-related rocks, and implications for hydraulic structure of fault zones

JAMES P. EVANS

Department of Geology, Utah State University, Logan, UT 84322-4505, USA

CRAIG B. FORSTER

Energy and Geoscience Institute, University of Utah, 423 Wakara Way, Salt Lake City, UT 84108, USA

and

JAMES V. GODDARD

Department of Geology, Utah State University, Logan, UT 84322-4505, USA. Present Address: CH2M Hill, 4001 South 700 East, Salt Lake City, UT 84107-2177, USA

(*Received* 10 *January* 1997; *accepted in revised form* 30 *July* 1997)

Abstract—The permeability structure of a fault zone in granitic rocks has been investigated by laboratory testing of intact core samples from the unfaulted protolith and the two principal fault zone components; the fault core and the damaged zone. The results of two test series performed on rocks obtained from outcrop are reported. First, tests performed at low confining pressure on 2.54-cm-diameter cores indicate how permeability might vary within different components of a fault zone. Second, tests conducted on 5.1-cm-diameter cores at a range of confining pressures (from 2 to 50 MPa) indicate how variations in overburden or pore fluid pressures might influence the permeability structure of faults. Tests performed at low confining pressure indicate that the highest permeabilities are found in the damaged zone (10^{-16}–10^{-14} m^2), lowest permeabilities are in the fault core ($<10^{-20}$–10^{-17} m^2), with intermediate permeabilities found in the protolith (10^{-17}–10^{-16} m^2). A similar relationship between permeability and fault zone structure is obtained at progressively greater confining pressure. Although the permeability of each sample decays with increasing confining pressure, the protolith sustains a much greater decline in permeability for a given change in confining pressure than the damaged zone or fault core. This result supports the inference that protolith samples have short, poorly connected fractures that close more easily than the greater number of more throughgoing fractures found in the damaged zone and fault core. The results of these experiments show that, at the coreplug scale, the damaged zone is a region of higher permeability between the fault core and protolith. These results are consistent with previous field-based and *in-situ* investigations of fluid flow in faults formed in crystalline rocks. We suggest that, where present, the two-part damaged zone–fault core structure can lead to a bulk anisotropy in fault zone permeability. Thus, fault zones with well-developed damaged zones can lead to enhanced fluid flow through a relatively thin tabular region parallel to the fault plane, whereas the fault core restricts fluid flow across the fault. Although this study examined rocks collected from outcrop, correlation with *in-situ* flow tests indicates that our results provide inexact, but useful, insights into the hydromechanical character of faults found in the shallow crust. © 1997 Elsevier Science Ltd.

INTRODUCTION

Faults profoundly affect patterns and rates of fluid flow in both modern and paleo-flow systems found in the upper part of the Earth's crust. Metoric water and deep-level fluids may penetrate and influence rocks at depths as deep as 10 km (e.g. Nesbitt and Muehlenbachs, 1989) and in flow regimes operating on scales ranging from the microscale to basins tens of kilometers wide (Bethke, 1985; Ge and Garven, 1994). Fault zones act as barriers, conduits, or mixed conduit/barrier systems, which form important components of fluid flow regimes operating in the upper crust (Smith *et al.*, 1990; Antonellini and Aydin, 1994; Caine *et al.*, 1996). As a fault evolves, its structure and hydraulic properties may vary over time and space (Smith, 1980; Allan, 1989; Bouvier *et al.*, 1989; Pittman, 1981; Smith *et al.*, 1990; Knipe, 1992; Harding and Tuminas, 1988; Bouvier *et al.*, 1989; Anderson *et al.*, 1994). Some faults formed conduits early in their histories (Gibson, 1994; Roberts, 1995; Anderson, 1995; Tellam, 1995) only to become barriers to fluid flow later in their history. The impact of fault-related compartmentalization and permeability anisotropy on fluid flow has been documented at the small scale (Randolph and Johnson, 1989; Mozley and Goodwin, 1995; Ashland *et al.*, 1996), and at the aquifer scale (Kastning, 1977; Huntoon, 1987; Maclay and Groschen, 1992; Maclay and Small, 1983). Numerical models incorporating fault-like features illustrate how faults may act as barriers or conduits to fluid flow and influence fluid pressure distributions (Forster and Smith, 1988; Bernard *et al.*, 1989; Forster and Evans, 1991; Lopez *et al.*, 1994; Lopez and Smith, 1995; Haneberg, 1995) and the stresses on the fault (Barton *et al.*, 1995). Few quantitative data are available, however, to provide geologically plausible permeability

values for faults and fault-like features incorporated in numerical simulators.

Quantitatively assessing the impact of fault zones on fluid flow in modern and paleo-flow systems requires an accurate conceptual model of fault zone structure coupled with sound data regarding the hydraulic properties of different fault zone components. Field and microstructural studies of fault zones demonstrate that fault zones are composed, in varying amounts, of two principal components (Chester and Logan, 1986; Caine *et al.*, 1996): the damaged zone (a region of enhanced subsidiary fracturing, faulting, and veining) and the fault core (fine-grained incohesive to well-indurated fault gouge or cataclasite). These principal fault zone components are encompassed by the protolith, or undeformed host rock. The amount and distribution of each component depend upon the lithology and geologic setting within which the fault has formed (Caine *et al.*, 1996). Boundaries between the damaged zone and fault core are typically sharp, whereas the damage zone to protolith transition is usually gradational (Caine *et al.*, 1996).

Few studies have systematically examined the permeability characteristics of different fault components. Antonellini and Aydin (1994) report that cataclastic deformation may reduce sandstone permeabilities by as much as 10^4 (to 10^{-19}–10^{-16} m^2) within carefully described, fine-grained deformation bands. Davison and Kozak (1988) note that *in-situ* permeabilities measured within a small thrust fault in crystalline rocks range from 10^{-17} to 10^{-11} m^2 without identifying how the permeability structure might relate to structural elements of the fault. Many laboratory-based permeability measurements have been performed on reconstituted fault gouge derived from crystalline rocks (Morrow *et al.*, 1981, 1984; Morrow and Byerlee, 1988; Chu and Wang, 1988; Faulkner and Rutter, 1996). The low permeabilities obtained in these tests (10^{-22}–10^{-19} m^2) are likely to be representative of the fault-core component of a fault zone developed in crystalline rocks, although the work of Faulkner and Rutter (1996) documents an orientation effect on the permeability values within the fine-grained gouge. Additional permeability-shear experiments using artificial gouge in sandstone rocks show that increasing shear strain leads to permeability reduction in fault gouge (Teufel, 1987) but yields little insight into the way that the permeability might vary as a function of shear strain within the damaged zone. A large number of laboratory tests performed on fractured rocks obtained from both faulted and unfaulted environments show that permeability declines with increasing confining pressure in samples containing either single or multiple fractures (Brace *et al.*, 1968; Brace, 1978; Kranz *et al.*, 1979; Walsh, 1981; Morrow *et al.*, 1984; Bernabe, 1986; Lin *et al.*, 1986; Morrow and Byerlee, 1992; Frederich *et al.*, 1993; Morrow and Lockner, 1994; Morrow *et al.*, 1994). Little information is available, however, to determine how pressure-permeability relationships might vary in the different fault components.

This paper presents the results of a study designed to determine how the permeability structure of a fault zone can be related to the consequences of fault evolution. We present experimentally determined permeabilities of natural, fault-related rocks developed in granitic gneisses. Representative samples of protolith, damaged zone, and fault-core rocks collected from outcrop are included in the sample set. Pressure-permeability relationships have been evaluated by measuring permeabilities across a range of confining pressures (0–50 MPa). A preliminary effort is made to estimate how preferred orientations of structural fabrics and fracture networks might lead to permeability anisotropy within a fault. The test results are interpreted in light of our previous work on the microstructures of the fault-related rocks and in terms of our present understanding of fault zone growth processes.

The determination of physical properties of exhumed fault-related rocks has two caveats. The permeabilities of rocks obtained from outcrop are commonly different from values obtained from drill holes (Morrow and Lockner, 1994). The permeability of exhumed samples tends to display less pressure sensitivity, perhaps due to the the presence of weathering products in fractures on the outcrop samples. Secondly, tests on samples from any fault zone represent only one stage on the temporal evolution of the fault, and in faults that are no longer active, from a 'dead' system. None the less, we have little opportunity to examine the real-time change in fault zone permeability, and testing of 'dead' systems still provides an insight into the differences between fault zone components and the properties of fault zones during their interseismic phase.

GEOLOGIC SETTING OF ROCKS EXAMINED

Samples used in the testing program were collected from outcrops of one of the East Fork thrust faults found in the Washakie Range, Wyoming, U.S.A. The East Fork thrust faults are hanging wall imbricates of the EA thrusts (Evans, 1993), which are a series of moderately dipping reverse faults that juxtapose Precambrian granite and gneiss on Paleozoic and Mesozoic sedimentary rocks of the Wind River basin. Fault zones in the East Fork area formed at depths of 4–7 km have granite and gneiss in both the footwall and hanging wall, and have 2–4 km of slip (Evans, 1993). Quartz veins, iron-oxide-filled fractures, and syntectonically altered feldspar grains indicate that fluid infiltrated the fault zone during slip (Evans, 1990).

Two fault types are found in the East Fork fault zone; narrow faults (2–4 cm thick) comprising clay-rich foliated cataclasites and wider (up to 20 cm thick) indurated gouge zones. Damaged zones consist of irregularly shaped regions of enhanced fracturing, faulting, and veining, which bound the fine-grained cataclasites. The damaged zones give way to protolith quartz

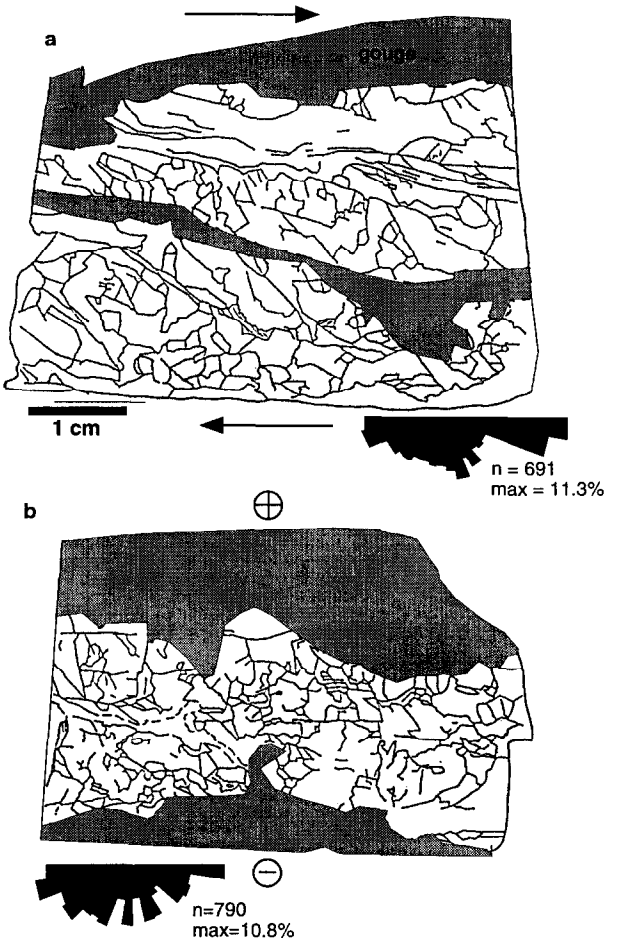

Fig. 1. Fabrics of microfractures as a function of sample orientation. (a) View of a core plug cut perpendicular to the fault slip vector and viewed parallel to the fault strike. Samples viewed perpendicular to the slip vector, in the strike direction of the fault, exhibit a larger number of fractures oriented at 0–20° to the fault surface than sampled viewed down the fault dip. Fracture densities are shown by rose diagrams of fracture orientations for three samples, with largest petal equal to 11.3% of total population, and other petals scaled accordingly. Shaded regions are fault gouge. Sense of slip shown by arrows. The tendency for fractures to form subparallel to the fault plane leads to an effective permeability at the core plug scale with reduced permeability normal to the fault plane. (b) View of a core plug cut parallel to the fault slip vector (looking down the fault dip). Top towards viewer. Fracture orientations are distributed more uniformly in this view when compared to that shown in (a). At the coreplug scale, this likely produces an approximately isotropic permeability tensor within the viewing plane.

diorite gneisses, which have little grain scale deformation, but do exhibit fractures spaced 0.25–2 m, with a variety of orientations (Evans, 1993; Evans *et al.*, 1993). Contacts between the fine-grained faults and the damaged zones are sharp, whereas contacts between the damaged zones and the protolith are gradational. The dominant deformation mechanisms included brittle inter- and intragranular fracture and comminution of feldspars and quartz (Evans, 1988, 1990). Subsequent to brittle deformation, syntectonic alteration of feldspars to clays resulted in development of foliated cataclasites.

Microstructural studies (scales of observation from several mm to 6 cm) of the rocks from the East Fork fault zone (Evans, 1990; Goddard and Evans, 1995) show that the damaged zone and fault core rocks exhibit a preferred orientation of fractures and fabric elements that probably leads to an inherent permeability anisotropy within these fault components. For example, damaged zone thin sections cut in a vertical plane parallel to transport (slip) direction and perpendicular to the fault surface (Fig. 1a) show a modest to strong preferred orientation of transgranular fractures between 0° and 20° to the plane of the fault, whereas vertical thin sections cut perpendicular to the slip vector reveal that the damaged zone samples have a blocky fracture pattern (Fig. 1b). The frequency of fractures subparallel to the fault, as viewed parallel to fault strike is much greater than when viewed downdip (Fig. 1b), and the total fracture lengths are greater in the orientations subparallel to the main slip surfaces. Intragranular fractures tend to be controlled by the orientations of the two prominent cleavages in feldspar (Evans, 1988). Fabric elements of the fault core samples are composed of clay-rich zones and slip surfaces that are almost parallel to the boundaries of the faults as viewed in both planes. The microstructural studies also show that microfracture densities in the damaged zone are three to five times greater than in the protolith (Evans, 1988). These microstructural studies document that fabrics of the fault core rocks formed during faulting. Exhumation may have altered the fracture densities in the rocks. Thus, our results are strictly applicable in the upper 2–3 km of crust, over the range of confining pressures used.

EXPERIMENTAL CONDITIONS

Thirty-one core samples were selected, at a variety of orientations relative to the slip plane (Fig. 2), to provide test results representing the primary components of fault-related rocks from the East Fork fault (gouge, damage zone, and adjacent protolith). Two core sizes were tested; 2.54 cm (1 inch) and 5.08 cm (2 inch) in diameter. Sample lengths are generally at least twice the sample diameter. Samples were cored in the laboratory from approximately rectangular blocks of fault-related rocks collected in the field. Block sizes varied from 20 to 45 cm on a side. Both ends of each core sample were ground flat and parallel, and the core was dried at a temperature of 105°C. Samples were jacketed in heat-shrink tubing and capped at each end before being submerged in the confining fluid of the hydrostatic test cell. All tests were performed by Terra Tek, Inc. in their Salt Lake City laboratory using equipment designed by Terra Tek. Equipment limitations preclude measuring permeabilities less than 10^{-20} m^2.

The smaller cores (19 in number) were tested using a nitrogen gas permeant at room temperature with a single effective confining pressure (P_c) of 3.5 MPa, a pore pressure (P_p) of 1.3 MPa, and a steady state method. A steady flow field is maintained in the sample using an upstream constant flow pump while the downstream end

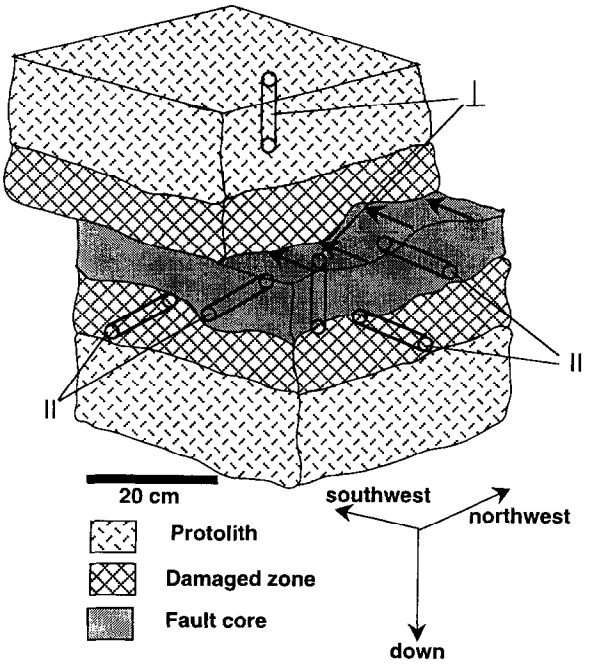

Fig. 2. Schematic block diagram showing the orientation of cored samples and the fault rock components sampled in this study. Arrows indicate slip direction of fault.

is vented to the atmosphere. Differential pressures are measured between the upstream and downstream ends. The larger cores (12 in number) were tested at room temperature using nitrogen gas and a transient pressure pulse method. The larger cores were each subjected to a series of confining pressures ranging from 2 to 47 MPa (with pore pressures fixed at about 2.7 MPa) to evaluate how the permeability of each fault component might vary during deformation or as a function of depth. Because the smaller samples were collected in sets of three mutually-perpendicular orientations relative to the slip plane (Fig. 2), these test results provide an insight into the orientation and magnitude of permeability anisotropy that might be found within each fault component. These results should prove useful for estimating the *in-situ* permeability structure of faults encountered in shallow investigations.

Equipment limitations preclude testing with pore pressures maintained at a constant deviation from the applied confining pressure. Thus, test results obtained with confining pressures above about 10 MPa are 'under-pressured' relative to typical *in-situ* fluid pressure conditions. That is, when applied confining pressures exceed 10 MPa, the effective stress (P_e) on the sample exceeds that which would be expected where *in-situ* confining stresses and pore fluid pressures, respectively, reflect typical lithostatic and hydrostatic gradients. As a consequence, permeability values obtained at confining pressures in excess of 10 MPa may underestimate the *in-situ* permeabilities that might be associated with each sample. Despite this limitation, however, the relative variations in permeabilities obtained at high confining pressure may still provide reasonable insight into the permeability variations found within and between each fault component.

Testing these relatively small samples yields a biased view of the bulk permeability of the faulted and fractured rock mass because the larger fractures are not included in the core plugs. Thus, each test result probably underestimates the bulk permeability of a larger volume of rock than that tested in the laboratory. The bias is minimized where fractures are more widely spaced (e.g. in the fault core and protolith) and maximized where fracturing is more intense (e.g. in the damage zone). The magnitude of the bias inherent in using small core samples is best evaluated through a comprehensive program of *in-situ* testing within a larger volume of rock that includes a more representative number of through-going fractures.

RESULTS

Results of the laboratory tests illustrate variations of permeability in three categories:

(1) between the different fault-related components; fault core, damaged zone, and protolith,

(2) as a function of orientation relative to fault slip within a specific fault component, and

(3) as a function of confining pressure. Low P_c test results obtained for the small diameter samples range from less than 10^{-20} m^2 (lower limit of the test apparatus) to 2×10^{-15} m^2 (Table 1 and Fig. 3). Samples from the damaged zone fall in the highest range of permeability (10^{-16}–10^{-14} m^2), whereas fault core samples have permeabilities in the lowest range ($<10^{-20}$–10^{-17} m^2). Protolith samples fill a narrow, intermediate, range of permeability between 10^{-18} m^2 and 10^{-17} m^2. Thus, at low effective stresses ($P_e = P_c - P_p$), the permeability of fault-related rocks depends strongly on the sample position within the fault zone. Similar results are obtained as the effective confining pressure applied to the sample is increased (Fig. 4). At the relatively small scale of these tests (2.5- and 5.4-cm-diameter core plugs), there may be a 10–10^4 contrast in permeability between damaged zone and protolith, and a similar contrast between the damaged zone and fault core samples. Several of the fault core samples exhibit such low permeabilities that a contrast of up to 10^6 is possible between damaged zone and fault core. Thus, the gouge/cataclasite component may hinder fluid flow across the fault while the damaged zone may enhance flow within the plane of the fault.

Tests performed at a low confining pressure on the 2.5-cm diameter cores reveal a distinct orientation dependence of permeability with anisotropy ratios as high as 10^4. Samples of fault core oriented parallel to the fault plane (Fig. 1) have permeabilities in the range of 10^{-18}–10^{-17} m^2 (Table 1), whereas samples oriented perpendi-

Table 1. Laboratory estimates of permeability of 2.54-cm-diameter core at 3.4 MPa net effective stress

Sample type	Sample number	Orientation	Permeability (m^2)
Protolith	EF391-A	Par 2	9.8×10^{-17}
	EF391-B	Par 2	1.8×10^{-17}
	EFR		2.2×10^{-16}
	EFY		1.4×10^{-16}
Damaged Zone	EF291-B	Par 2	1.4×10^{-16}
	EF391-C	Par 2	1.9×10^{-16}
	EF591-A	Par 1	1.9×10^{-15}
	EF591-B	Par 1	1.6×10^{-15}
	EFP1	Par 1	1.2×10^{-15}
	EFP2	Par 1	3.0×10^{-15}
Gouge/Cataclasite Zone	EF291-V	Perp	1.3×10^{-17}
	EF591-V	Perp	$< 10^{-20}$
	EF391-V	Perp	9.6×10^{-19}
	EFV	Perp	2.0×10^{-17}
	—	—	—
	EF291-A	Par 2	4.5×10^{-18}
	EF291-C	Par 2	8.0×10^{-18}
	EF591-C	Par 1	7.4×10^{-17}
	EFH1	Par 1	6.0×10^{-17}
	EFH2	Par 1	1.0×10^{-17}

Orientation notation: Perp: perpendicular to the fault plane; Par 1: parallel to the fault plane and parallel to slip direction; Par 2: parallel to fault plane and perpendicular to fault slip.

cular to the fault plane have values ranging from less than 10^{-20} to 10^{-17} m^2. Although samples were unavailable to assess permeability normal to the fault within the damage zone and protolith, data shown in Table 1 suggest that permeability anisotropy may occur within the plane of the fault in both the damage zone and protolith. In each case, the permeability of samples oriented parallel to the slip vector is about one order of magnitude greater than that of samples oriented perpendicular to slip. This limited data set suggests that each component of the fault zone may exhibit three-dimensional permeability anisotropy with minimum permeability values perpendicular to the fault plane, maximum values parallel to the slip vector, and intermediate values within the fault plane but perpendicular to slip. Although sample orientation relative to the orientation of the fault plane appears to have influenced the permeabilities measured at low confining pressure in the smaller diameter samples, an insufficient number of larger diameter samples are available to determine whether an orientation effect persists across a range of applied effective stresses. Additional studies are required to more fully evaluate this hypothesis, test the possibility that it might hold in other fault environments, and assess the implications of permeability anisotropy in engineering applications.

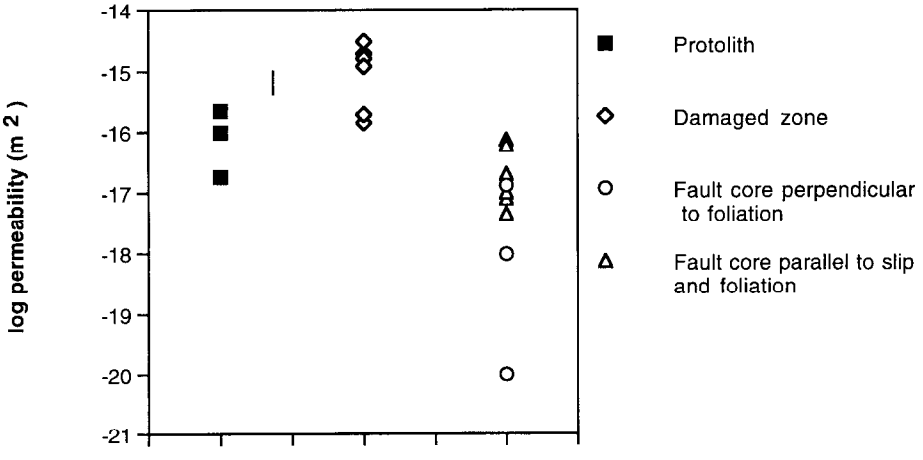

Fig. 3. Results of permeability tests performed at low confining pressure as a function of structural position within the fault zone. Protolith permeabilities are typically lower than those of the damaged zone and greater than those of the fault core. Samples cored in the fault plane yield higher permeabilities than samples cored normal to the fault plane. The small bar indicates the approximate measurement error.

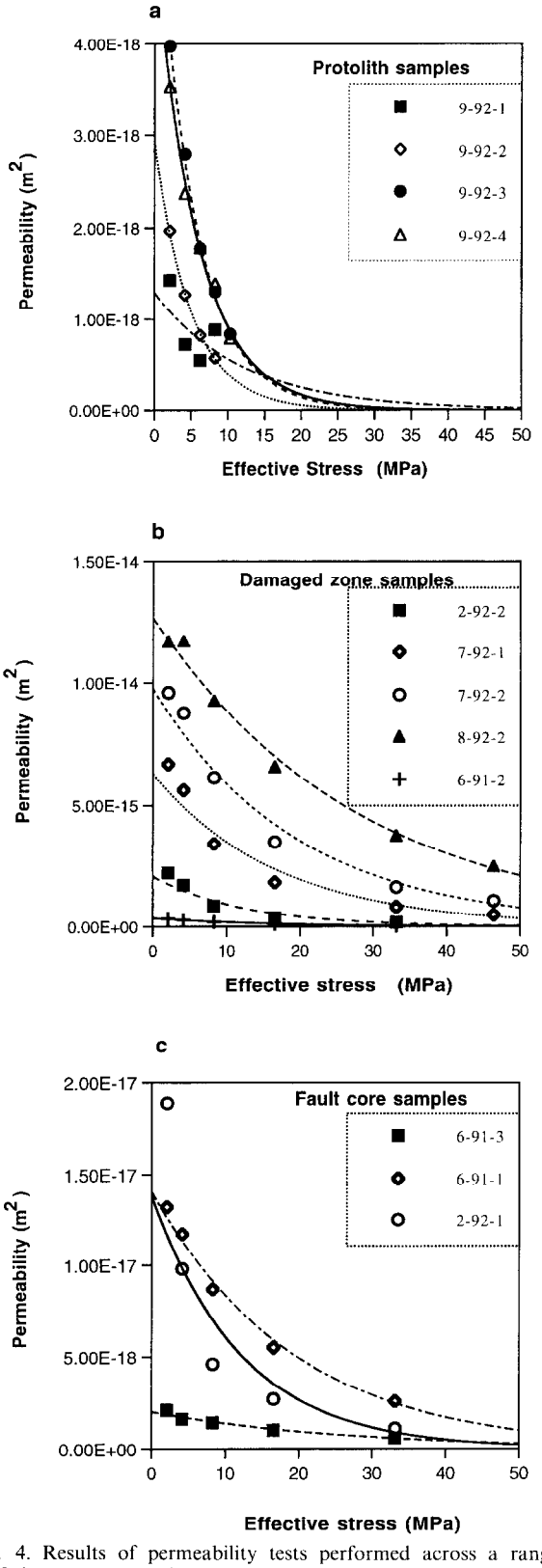

Fig. 4. Results of permeability tests performed across a range of confining pressures. The abscissa is scaled the same in each panel; however, the ordinate scaling varies from panel to panel. (A) Protolith samples exhibit a relatively steep decline in permeability with small increases in net effective stress. Initial permeabilities are less than 1×10^{-18} m^2 at effectives stresses of 5–10 MPa. (B) Damaged zone samples yield higher initial permeabilities and exhibit shallow declines in permeability with large increases in net effective stress. (C) Fault core samples yield low initial permeabilities and exhibit moderate declines in permeability with large increases in net effective stress.

These results agree reasonably well with conceptual models for fault-zone permeability structure (Scholz, 1994; Caine *et al.*, 1996), with *in-situ* tests performed at a shallow depth (Davison and Kozak, 1988; Andersson *et al.*, 1991), with observations in underground mines (Martel and Peterson, 1991; Lachmar, 1994; Levens *et al.*, 1994) and with observations made during tunneling through fault zones (Schadt, 1905; Fox, 1907; Mears, 1932). These studies show that shallow faults can contain a zone of relatively high permeability that forms a crudely planar conduit within the fault while a zone of relatively low permeability restricts fluid flow across the fault. The tunnel driving observations provide a particularly graphic illustration of this effect because water trapped in a zone of high permeability within the fault plane is often released at high flow rate over a short term when a tunnel penetrates the adjacent zone of much lower permeability (Mears, 1932). Although detailed information is often lacking to conclude definitively that all high permeability features found within a fault zone correspond to a damaged zone (and lower permeability features correspond to gouge or cataclasite), our studies of a number of faults suggest that this may often be the case.

Tests performed at a series of progressively more elevated confining pressures show how the permeability of each component type might respond to deformation caused by increased overburden stress or reduced pore fluid pressure (Fig. 4 and Table 2). Plotting permeability as a function of P_c reveals a decline in permeability with increasing P_c that differs for each component type (Fig. 4). The general form of the permeability decay curves is similar to those observed in previous tests of intact samples (Brace *et al.*, 1968; Brace, 1978; Kranz *et al.*, 1979; Bernabe, 1986; Frederich *et al.*, 1993), in single fracture samples (Kranz *et al.*, 1979; Walsh, 1981) and in fault gouge tests (Morrow *et al.*, 1984). Our test results show three important results:

(1) permeability decays exponentially with P_c,
(2) permeability of the damaged zone is 10–1000 times greater than samples from the protolith or fault core, and permeability in the damaged zone samples drops off more slowly with P_c than do samples from the protolith or fault core, and
(3) differences between hydromechanical properties of the fault component types decreases with increased P_c.

The best-fit relationship between permeability and effective stress are shown in Fig. 4 and have an exponential form:

$$K = K_0 \exp(-\gamma P_c),$$

where

K = the permeability at effective stress P_c,
K_0 = the sample permeability when $P_c = 0$, and
γ = a curve fitting parameter, which is a measure of the dependence of K on the effective stress.

Table 2. Permeability at effective stresses for 5.2-cm-diameter cores

Sample type	Sample number	Orientation	Ambient porosity (%)	Permeability (m^2) at Net effective stress/M PA 2.07	4.14	8.274	16.55	33.10	46.89
Cataclasite	2-92-1	Par 2	1.946	1.89×10^{-17}	9.80×10^{-18}	4.62×10^{-18}	2.72×10^{-18}	1.13×10^{-18}	N/A
Damaged Zone	2-92-2	Par 1	2.081	2.23×10^{-15}	1.713×10^{-15}	8.52×10^{-17}	3.74×10^{-16}	1.77×10^{-16}	N/A
Damaged Zone	7-92-1	Par 1	3.448	6.69×10^{-15}	5.63×10^{-15}	3.43×10^{-15}	1.84×10^{-15}	3.08×10^{-16}	4.9×10^{-16}
Damaged Zone	7-92-2	Par 2	3.706	9.60×10^{-15}	8.78×10^{-15}	6.15×10^{-15}	3.51×10^{-15}	1.64×10^{-15}	1.07×10^{-15}
Damaged Zone	8-92-2	Par 1	2.963	1.168×10^{-14}	1.17×10^{-14}	9.27×10^{-15}	6.58×10^{-15}	3.76×10^{-15}	2.5×10^{-15}
Cataclastic	6-91-1	Perp	1.679	1.32×10^{-17}	1.16×10^{-17}	8.67×10^{-18}	5.58×10^{-18}	2.59×10^{-18}	N/A
Damaged Zone	6-91-2	Par 2	2.239	3.32×10^{-16}	2.93×10^{-16}	1.99×10^{-16}	1.08×10^{-16}	4.64×10^{-17}	N/A
Cataclastic	6-91-3	Perp	1.974	2.18×10^{-18}	1.63×10^{-18}	1.45×10^{-18}	1.03×10^{-18}	6.09×10^{-19}	N/A

Sample type	Sample number	Orientation	Ambient porosity (%)	Permeability (m^2) at Net effective stress (psi)/M PA 2.07	4.14	6.21	8.274	10.34
Protolith	9-92-1	Par 1	0.185	1.426×10^{-18}	7.27×10^{-19}	5.49×10^{-19}	8.863×10^{-19}	N/A
Protolith	9-92-2	Par 2	0.143	1.970×10^{-18}	1.27×10^{-18}	8.27×10^{-19}	5.704×10^{-19}	N/A
Protolith	9-92-3	Perp	0.299	3.975×10^{-18}	2.80×10^{-18}	1.77×10^{-18}	1.300×10^{-18}	8.40×10^{-19}
Protolith	9-92-4	Perp	0.263	3.530×10^{-18}	2.37×10^{-18}	1.78×10^{-18}	1.393×10^{-18}	7.95×10^{-19}

Orientation notation: Perp: perpendicular to the fault plane; Par 1: parallel to the fault plane and parallel to slip direction; Par 2: parallel to fault plane and perpendicular to fault slip.

Values of K_0 and γ computed for each sample are summarized in Table 3. For all three component types, the decay of permeability as a function of effective stress is notably similar to work on intact and fractured crystalline rocks (e.g. Brace and Martin, 1968; Kranz *et al.*, 1979; Bernabe, 1986; Frederich *et al.*, 1993; David *et al.*, 1994). Also similar is the decreased dependence of permeability on effective stress as the confining pressures increase (see Kranz *et al.*, 1979).

Values of K_0 clearly show that each fault component type has a characteristic maximum permeability K_0; the damaged zone has the highest values (about 10^{-15} m^2), the fault core has the intermediate values (about 10^{-17} m^2), and the protolith has low values of K_0 (about 10^{-18} m^2). Although values of γ are similar for both damaged zone and fault core (0.04–0.08 MPa^{-1}), the protolith has notably larger values (about 0.20 MPa^{-1}). David *et al.* (1994) have compiled experimentally derived values of γ for a variety of rock types. Intact gneiss and granites have γ of 0.023–0.032 MPa^{-1} (Bernabe, 1986; Kranz *et al.*, 1979), and 0.058–0.11 MPa^{-1} for amphibolite (Morrow *et al.*, 1994). Our results from the damaged zone are close to those determined in fractured granitic rocks (0.079–0.092 MPa^{-1}, Kranz *et al.*, 1979), and for clay-rich fault gouge (0.012–0.055 MPa^{-1}; Morrow *et al.*, 1984). Larger values of γ correspond to a strong response to changes in effective stress (David *et al.*, 1994). Previous work suggests that the permeability reduction that occurs in samples with large values of γ probably results from crack closure (David *et al.*, 1994). In general, all values for γ are smaller than the 0.2 MPa^{-1} value used by Rice (1992) in modeling the pore pressure near a fault zone.

Table 3. Curve-fitting parameters for the data in Fig. 4

Rock type	K_0 (m^2)	γ (MPa^{-1})
Protolith	5.03×10^{-18}	0.165
	1.29×10^{-18}	0.200
	2.93×10^{-18}	0.187
	5.92×10^{-18}	0.170
Damaged Zone	2.08×10^{-15}	0.082
	6.28×10^{-15}	0.059
	9.73×10^{-15}	0.051
	1.26×10^{-14}	0.035
	3.57×10^{-16}	0.062
Fault core	1.38×10^{-17}	0.082
	1.41×10^{-17}	0.052
	2.04×10^{-17}	0.038

Comparison of the results obtained for each component type is complicated by the fact that permeabilities associated with each component can differ from other components by at least one order of magnitude. Thus, we plot normalized permeability as a function of P_e to explore variations in the hydromechanical response of each component to changes in confining pressure (Fig. 5). Normalized permeability varies from 0 to 1 and is computed separately for each sample. In each case, the maximum value of K (corresponding to the minimum P_e) obtained for the sample is used to normalize the results obtained at successively higher values of P_e.

The normalized permeability vs effective stress plots shown in Fig. 5 highlight the contrast between the hydromechanical response of the protolith and the response of both the damaged zone and fault core. For example, the permeability of the protolith samples is reduced to approximately 10% of the initial value at an applied effective stress of about 12 MPa. Much larger applied stresses (30–50 MPa) are required, however, to reduce the permeability of the other fault components.

The dramatic drop in permeability obtained for the

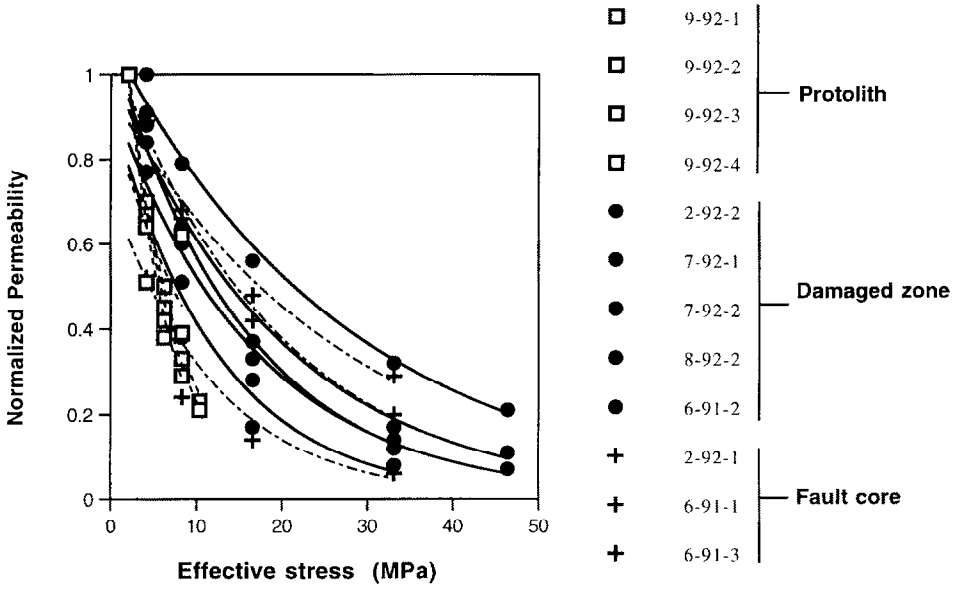

Fig. 5. Normalized permeability as a function of confining pressure. Increasing effective stress causes a sharp decline in protolith permeability, whereas a much shallower decline is found for both the damaged zone and fault core samples.

protolith over a small range of confining pressure (Figs 4 & 5) corresponds to the larger values of γ shown in Table 3. We interpret these data as reflecting a low initial fracture density and high sample stiffness in the protolith that, in turn, contribute to hydrostatic compaction due to crack closure. The more shallow decline in permeability seen in the fault gouge samples is attributed to a low initial permeability that is further reduced by grain rearrangement and flattening. The foliated cataclasites tested here are fine-grained and fractured, and exhibit higher permeabilities than the protolith. Changes in P_c do not significantly alter K vs P_e behavior, as there are few cracks to be closed in these rocks, and the permeability may be intergranular.

The pressure sensitivity of protolith vs the relative lack of sensitivity in the damaged zone samples may also be due to the effects of weathering. Rocks with greater densities of fractures are likely to have more weathering products, which appears to reduce the pressure sensitivity of permeability (Morrow and Lockner, 1994), whereas the protolith samples are less likely to have weathered along tectonically developed fractures, and thus have a higher pressure sensitivity.

The mechanical behavior in rocks subjected to changes in either confining pressure or pore fluid pressure has commonly been cast in terms of the effective stress relationship (Hubbert and Rubey, 1959; Handin *et al.*, 1963; Brace, 1972) where the effective stress, P_e, is given by:

$$P_e = P_c - P_p.$$

In many porous, permeable rocks, this relationship appears to be valid (Handin *et al.*, 1963; Garg and Nur, 1973). However, a more general expression for the static case is:

$$P_e = P_e - \alpha P_p$$

(Nur and Byerlee, 1971; Robin, 1973; Garg and Nur, 1973; Zoback and Byerlee, 1975; Kranz *et al.*, 1979; Walsh, 1981), where the factor α depends on rock type, fracture topography and connectivity, porosity, pore geometry, and tortuosity (Kranz *et al.*, 1979; Walsh, 1981; Bernabe, 1986; Berryman, 1992). The value of α is found empirically, and can range from 0 to 1.0 for fractured and intact rocks. Values of α less than 1 obtained for intact crystalline rocks have been ascribed to microfracture dilatency (Brace and Martin, 1968), in which the true internal pore pressures differ from the externally measured pore pressures. For experiments conducted on single fractures (Kranz *et al.*, 1979), Walsh (1981) showed that the value of α was 0.5–0.7. Morrow *et al.* (1994) showed that α is 1.0 for friction experiments on montmorillonite/illite gouges in drained conditions, whereas α is much less than 1.0 in undrained friction experiments with clay or sheet silicate gouges (Morrow *et al.*, 1984).

In order to determine α, permeability tests must be run at a variety of P_p and P_c values. Since the experiments reported here were conducted at a single value of P_p, we cannot explicity find α. However, we can compare the results shown in Figs 4 and 5 with the interpretations of Walsh (1981) to estimate crudely how α might vary as a function of fault rock type. We infer that α is higher for damaged zone samples and lower on the fault core and protolith samples. The higher fracture densities and larger degree of fracture interconnectivity may create a rock that is closer to a porous, permeable rock that can transmit fluids and fluid pressures effectively, and thus the value of α would be closer to 1.0. The low fracture densities and fine-grained nature of the protolith and

fault core may result in a significant departure from the ideal effective stress relationship, and would yield α values much lower than 1.0.

DISCUSSION

Our work examines the coreplug-scale permeability of samples of fault-related rocks in granitic gneisses collected from outcrop, which represent one stage of fault development. As such, the numerical values reported here, and in many other tests of permeability, can be strictly applied to a narrow range of natural analogs. Permeabilities associated with a particular rock type or fault zone component likely vary as a function of the sample size tested. Brace (1984) and Clauser (1992) outline how the increase in fracture intensity and connectivity associated with increasing sample size (from lab to well-test scales) produces an apparent increase in bulk permeability. Given the problems of the scale effect, exhumation, and temporal evolution of faults, we discuss how our coreplug-scale tests aid in understanding the permeability structure of individual fault zone components, then attempt to infer how these results provide insight into larger, fault-zone scale permeability structure both for modern flow systems with 'dead' faults, and in the evolutionary development of faults.

The coreplug-scale test results show a clear distinction between the relatively high permeability damaged zone and the lower permeability protolith and fault core. Enhanced permeability in damaged zones has implications for understanding the *in-situ* hydraulic properties and hydraulic structure of faults. The test results suggest that damaged zones, where present, would form pathways for enhanced fluid flow. This inference is supported by geochemical, petrologic, and mineralogic studies of the fault zone. Goddard and Evans (1995) and Evans (1988, 1990), show that damaged zones found in the East Fork faults are zones of increased mineralogic alteration to hydrous clays, increased vein abundances, and variations in the elemental composition of the rocks as compared to the protolith. In addition, the damaged zones exhibit modest losses in soluble elements and slight increases in less soluble elements. Similar evidence for localized fluid flow in damaged zones has been documented in larger displacement faults found in crystalline rocks of the nearby Wind River Range (Goddard and Evans, 1995) and along the San Gabriel fault (Evans and Chester, 1995), and the Punchbowl fault (Chester and Logan, 1986). Fracture density, measured at the thin-section scale, is three to five times greater in the damaged zone than in the protolith (Evans, 1988). Thus, the permeability results presented here suggest a permeability structure for the fault zone that agrees with inferences based on fluid–rock interactions that occurred while the fault was active.

The permeability values determined here should be used with caution as a basis for developing quantitative models of fluid flow in faults. For example, values obtained for the damaged zone samples may be representative only of permeabilities associated with the relatively unfractured fault or fracture-bounded blocks used in a dual-permeability modeling approach. Thus, *in-situ* permeability tests aimed at determining the bulk permeability of the damaged zone would probably yield higher values because fractures not encountered at the coreplug scale will provide greater bulk connectivity. For example, *in-situ* tests performed in faulted crystalline rocks at the Canadian Underground Research Laboratory yield permeabilities that range from 10^{-17} to 10^{-11} m^2 (Davison and Kozak, 1988; National Research Council, 1996, pp. 479–492). Values obtained for the fault core, however, may be more representative of its bulk permeability because the reduced fracture intensity of the fault core is less likely to modify estimates of bulk permeability based on tests performed at the coreplug scale.

Examining the outcrop-scale structure of the East Fork fault zone, and the other fault zones in crystalline rocks, leads us to suggest that damaged zones are characterized by fractures, veins, and small faults that form blocks 10 cm to several meters on a side (Mitra, 1984; Evans, 1988; Bruhn *et al.*, 1994; Goddard and Evans, 1995). Because these fractures, faults, and veins commonly display enhanced alteration and deposition of hydrous minerals, they appear to have formed mesoscale conduits supplying fluids to intervening blocks in the damaged zone. While the intragranular, coreplug-scale permeabilities reported here may provide representative values for the intervening blocks, *in-situ* tests are required to understand better the overall permeability structure of the damaged zone. We suggest that the results of our coreplug-scale tests on damaged zone samples did not exceed 10^{-14} m^2 because we could not include the larger, more throughgoing fractures found *in situ*.

The presence of a relatively high permeability damaged zone has implications for the fluid pressure state near fault zones. Permeabilities above 10^{-21} m^2 would preclude development of fluid pressures in excess of hydrostatic (Brace, 1984), and thus, the values measured here suggest that such high values of P_p cannot develop in the damaged zone.

The abundance of clay and fine-grained cataclasites found in the fault core is likely to cause well-developed fault cores to act as barriers to fluid flow across faults. Thus, if the forces driving fluid flow are arranged so that cross-fault flow is favored, the hydraulic character of a relatively thin fault core may dominate the effective hydraulic properties of a fault. Fault cores in crystalline rocks are commonly narrow and homogenous zones of fine-grained comminuted cataclasite and clays that probably evolved from damaged zones formed at earlier stages in fault development (Chester and Logan, 1986). The homogeneous character of many fault cores probably reflects the large amounts of strain accommodated

along them (Mitra, 1984; Chester *et al.*, 1993; Goddard and Evans, 1995). This apparent homogeneity, combined with the relatively low intensity of fracturing in fault cores, suggests that the coreplug-scale permeabilities estimated in this study may be applicable throughout the fault core. As a consequence, in the absence of detailed structural information and taking into account the effects of sample size and the influence of exhumation, we infer that fault core materials may be characterized by the lower end of the permeability range (about 10^{-17}–10^{-18} m^2), whereas more heterogeneous damaged zone materials may be characterized by the wider range of higher permeabilities (10^{-16}–10^{-11} m^2).

Permeability variations observed within a fault zone provide a basis for inferring the overall hydraulic effect of a fault. Caine *et al.* (1996) indicate that the relative proportion of fault core and damaged zone, combined with a knowledge of the permeability of each fault component, may be used to estimate the local- to regional-scale hydraulic behavior of the faults. Modeling results presented by Forster and Evans (1991) suggest that fluid flow through the more widely spaced fracture networks that control regional-scale flow in crystalline terrain is little affected by the detailed permeability structure of a fault. The bulk permeability structure of the fault, however, controls whether or not the fault will perturb the regional-scale flow system by acting as a conduit or barrier. When a fault acts as a conduit, fluid moving through relatively widely spaced fractures in the protolith is fed to the fault zone and transmitted within the more intensely fractured and permeable damaged zone (Forster and Evans, 1991; Lopez and Smith, 1995).

The two-component fault zone structure described here clearly does not apply to all faults formed in all settings. Some faults, such as deformation bands in sandstones, lack damaged zones with enhanced permeability (Aydin, 1978; Antonellini and Aydin, 1994). Permeability reduction in clastic sediments commonly results from pore collapse, crushing, grinding and grain-size reduction of rigid grains (Aydin, 1978; Fowles and Burley, 1994; Antonellini and Aydin, 1995), and smearing, growth, and plastic deformation of clay in faults (Smith, 1980; Knott, 1993; Lindsay *et al.*, 1993; Gibson, 1994), which is often accompanied by little or no damaged zone development. Thus, the deformation band faults yield a distinctive network of fault-controlled fluid flow barriers within the more porous and permeable sandstones.

The hydraulic structure of a fault changes during evolution such that structures observed in the field, or inferred during earlier geologic times, reflect the integrated effect of fault growth processes. For example, process zones inferred to form at the tips of propagating faults (Pollard and Segall, 1987; Martel and Pollard, 1989; Scholz *et al.*, 1993) may become damaged zones as a fault evolves. The character of a damaged zone is likely to reflect the impact of repeated slip events and the wear processes that induce deformation in response to perturbations in geometry or local stresses along the fault (Scholz, 1990). The presence or absence, and inherent character, of a damaged zone depend upon a variety of factors that include: the mechanical properties of the rocks, fluid–rock interactions, total strain, deformation mechanisms, and fault geometry. Thus, predicting the hydraulic structure and fluid flow properties of fault zones requires an understanding of (1) the structural setting and evolution of the fault, (2) the hydrologic setting of the fault, and (3) the mechanical development of the fault.

CONCLUSIONS

Coreplug-scale permeability tests performed over a range of confining pressures show that the permeability of naturally faulted crystalline rocks varies as a function of structural location within a fault zone and confining pressure. Permeability tests performed at low confining pressure provide two major results. First, damaged zone samples yield permeabilities from 10^{-16} to 10^{-14} m^2. The greater number of fractures, faults, and veins found in the damage zone yield permeabilities as much as 10^4 times greater than values obtained for the protolith and fault core samples, even at the coreplug scale. Second, samples of fault core and protolith have similar, but lower coreplug-scale permeabilities (less than 10^{-20}–10^{-17} m^2).

Permeability tests performed across a range of confining pressure (3–50 MPa) yield additional insight into the hydromechanical properties of faulted rocks. Although all three fault components display a logarithmic or exponential permeability decay with increased confining pressure, distinct differences are found between the behavior of the protolith samples when compared to fault gouge and damaged zone samples. For example, protolith permeability declines one order of magnitude as the confining pressure is raised to 12 MPa. Much higher confining pressures (30–50 MPa) are required to cause the same order of magnitude reduction in the permeability of the damaged zone and fault core samples.

We extend our laboratory test results to enhance our understanding of the bulk fluid flow properties of natural fault zones by suggesting that faults in crystalline rocks may comprise one or two zone(s) of enhanced permeability sandwiched between lower permeability fault core and protolith. This permeability structure probably causes the more intensely fractured damaged zone to act as a conduit for fluid flow, whereas the lower permeability fault core is likely to inhibit fluid flow across the fault. Thus, the fault zone has a bulk permeability anisotropy with higher permeability parallel to the fault plane and reduced permeability normal to the fault. Although difficult to document, this bulk anisotropy is probably superimposed on a permeability anisotropy derived from the anisotropic fabrics and fracture networks found within each fault component. Because our

tests were performed at confining pressures less than 50 MPa, our results are strictly applicable only in the upper 2 km of the crust. Thus, these results may be of greatest interest to those studying geotechnical problems, water resources protection and development, geothermal production, and shallow resource extraction issues.

Acknowledgements—Support for this work came from National Science Grant EAR-90-05027 and U.S. Geological Survey NEHRP grant 1434-92-G-2184. Reviews by Stephen Cox and Rick Sibson are gratefully acknowledged, and field assistance was provided by K. Davis and D. Hinton. Discussions with Jonathan Caine were very helpful in this work.

REFERENCES

Allan, U. S. (1989) Model for hydrocarbon migration and entrapment within faulted structures. *American Association of Petroleum Geologists Bulletin* **73**, 803–811.

Anderson, R. N. (1995) Migration pathway for hydrocarbons within a fault zone conduit in the Eugene Island 330 field offshore Louisiana. *Geological Society of America Abstracts* **27**, A–329.

Anderson, R. N., Flemings, P., Losh, S. and Austin, J. (1994) Gulf of Mexico growth fault drilled, seen as oil, gas migration pathway. *Oil and Gas Journal* **94**, 97–104.

Andersson, J. E., Ekman, L., Nordqvist, R. and Winberg, A. (1991) Hydraulic testing and modelling of a low-angle fracture zone at Finnsjon, Sweden. *Journal of Hydrology* **126**, 45–77.

Antonellini, M. and Aydin, A. (1994) Effect of faulting on fluid flow in porous sandstones: petrophysical properties. *American Association of Petroleum Geologists Bulletin* **78**, 355–377.

Antonellini, M. and Aydin, A. (1995) Effect of faulting on fluid flow in porous sandstones: Geometry and spatial distribution. *American Association of Petroleum Geologists Bulletin* **79**, 642–671.

Ashland, F. X., Bishop, C. E., Lowe, M., and Mayes, B. H. (1996) The geology of Snyderville Basin and its relation to ground-water conditions. *Utah Geological Survey Open-File Report* **337**, 182 pp.

Aydin, A. (1978) Small faults as deformation bands in sandstone. *Pure and Applied Geophysics* **116**, 913–930.

Barton, C. A., Zoback, M. D. and Moos, D. (1995) Fluid flow along potentially active faults in crystalline rock. *Geology* **23**, 683–686.

Bernabe, Y. (1986) The effective pressure law for permeability in Chelmsford granite and Barre granite. *International Journal of Rock Mechanics Mineral Sciences and Geomechanical Abstracts* **23**, 267–275.

Bernard, D., Danis, M. and Quintard, M. (1989) Effects of permeability anisotropy and throw on the transmissivity in the vicinity of a fault: Hydrogeological regimes and their subsurface thermal effects. *American Geophysical Union Monograph* **47**, 119–128.

Berryman, J. G. (1992) Exact effective stress rules in rock mechanisms. *Physical Review A* **46**, 3307–3311.

Bethke, C. M. (1985) A numerical model of compaction-driven groundwater flow and heat transfer and its application to paleohydrology of intracratonic sedimentary basins. *Journal of Geophysical Research* **90**, 6817–6828.

Bouvier, J. D., Kaars-Sijjpesteijn, C. H., Kleusner, D. F., Onyejekwe, C. C. and Pal, R. C. V. D. (1989) Three-dimensional seismic interpretation and fault sealing investigations, Nun River field, Nigeria. *American Association of Petroleum Geologists Bulletin* **73**, 1397–1414.

Brace, W. F. (1972) Pore pressure in geophysics. In *Flow and Fracture of Rocks*, eds H. C. Heard, I. Y., Borg, N. L., Carter and C. B. Raleigh. American Geophysical Union Monograph **16**, pp. 265–273.

Brace, W. F. (1978) A note on permeability changes in geologic material due to stress. *Pure and Applied Geophysics* **116**, 627–633.

Brace, W. F. (1984) Permeability of crystalline rocks: new *in situ* measurements. *Journal of Geophysical Research* **89**, 4327–4330.

Brace, W. F. and Martin, R. J. (1968) A test of the law of effective stress for crystalline rocks of low porosity. *International Journal of Rock Mechanics Sciences and Geomechanical Abstracts* **5**, 415–426.

Brace, W. F., Walsh, J. B. and Frangos, W. T. (1968) Permeability of granite under high pressure. *Journal of Geophysical Research* **73**, 2225–2236.

Bruhn, R. L., Parry, W. T., Yonkee, W. A. and Thompson, T. (1994) Fracturing and hydrothermal alteration in normal fault zones. *Pure and Applied Geophysics* **142**, 611–643.

Caine, J. S., Evans, J. P. and Forster, C. B. (1996) Fault zone architecture and permeability structure. *Geology* **24**, 1025–1028.

Chester, F. M., Evans, J. P. and Biegel, R. L. (1993) Internal structure and weakening mechanisms of the San Andreas fault. *Journal of Geophysical Research* **98**, 771–786.

Chester, F. M. and Logan, J. M. (1986) Implications for mechanical properties of brittle faults from observations of the Punchbowl fault zone, California. *Pure and Applied Geophysics* **124**, 80–106.

Chu, C. L. and Wang, C. Y. (1988) Permeability and frictional properties of San Andreas fault gouge. *Geophysical Research Letters* **8**, 565–568.

Clauser, C. (1992) Permeability of crystalline rocks. *EOS, Transactions American Geophysical Union* **73**, 233–238.

David, C., Wong, T., Zhu, W. and Zhang, J. (1994) Laboratory measurement of compaction-induced permeability change in porous rocks: implications for the generation and maintenance of pore pressure excess in the crust. *Pure and Applied Geophysics* **143**, 425–456.

Davison, C. C. and Kozak, E. T. (1988) Hydrogeological characteristics of fracture zones in a granite batholith of the Canadian Shield. In *Proceedings of the Fourth Canadian/American Conference Hydrology*, eds B. Hitchon and S. Bachu, pp. 53–59. National Water Well Association.

Evans, J. P. (1988) Deformation mechanisms in granitic rocks at shallow crustal levels. *Journal of Structural Geology* **10**, 437–443.

Evans, J. P. (1990) Thickness–displacement relationships for fault zones. *Journal of Structural Geology* **12**, 1061–1066.

Evans, J. P. (1993) Deformation mechanisms and kinematics of a crystalline-cored thrust sheet: The Washakie thrust system, Wyoming. In *Basement Deformation in Rocky Mountain Foreland Structures*, eds C. J. Schmidt, R., Chase and E. A. Erslev. Geological Society of America Special Paper **280**, pp. 147–161.

Evans, J. P., DuBois, M. A., Batatian, D., Derr, D., Harlan, S., Malizzi, L., McDowell, R., Nelson, G., Parke, M., Schmidt, C. J. and Weberg, E. (1993). Mechanisms and mechanics of a Precambrian-cored fold and fault structure: Jakey's Fork, Wyoming. In *Basement Deformation in Rocky Mountain Foreland Structures*, ed. C. J. Schmidt, R., Chase and E. A. Erslev. Geological Society of America Special Paper **280**, pp. 163–176.

Evans, J. P. and Chester, F. M. (1995) Fluid–rock interaction and weakening of faults of the San Andreas system: inferences from San Gabriel fault-rock geochemistry and microstructures. *Journal of Geophysical Research* **100**, 13007–13020.

Faulkner, D. R. and Rutter, E. H. (1996) The permeability anisotropy of clay-bearing fault gouge and its implications for earthquake source mechanisms. *EOS, Transactions American Geophysical Union* **77**, F736.

Forster, C. B. and Evans, J. P. (1991) Fluid flow in thrust faults and crystalline thrust sheets: Results of combined field and modeling studies. *Geophysical Research Letters* **18**, 979–982.

Forster, C. B. and Smith, L. (1988) Groundwater flow systems in mountainous terrain 1. Numerical technique. *Water Resources Research* **24**, 999–1010.

Fowles, J. and Burley, S. (1994) Textures and permeability characteristics of faulted high-porosity sandstones. *Marine and Petroleum Geology* **11**, 608–623.

Fox, F. M. (1907) The Simplon tunnel. *Minutes of the Proceedings of the Institute of Civil Engineering* **168**, pp. 61–86.

Frederich, J. T., Greaves, K. H. and Martin, J. W. (1993) Pore geometry and transport properties of Fontainebleau sandstone. *International Journal of Rock Mechanics Mineral Science and Geomechanical Abstracts* **30**, 691–697.

Garg, S. K. and Nur, A. (1973) Effective stress laws for fluid-saturated porous rocks. *Journal of Geophysical Research* **78**, 5911–5921.

Ge, S. and Garven, G. (1994) A theoretical model for thrust-induced deep groundwater expulsion with application to the Canadian Rocky Mountains. *Journal of Geophysical Research* **99**, 13851–13868.

Gibson, R. G. (1994) Fault-zone seals in siliciclastic strata of the Columbus Basin, offshore Trinidad. *American Association of Petroleum Geologists Bulletin* **78**, 1372–1385.

Goddard, J. V. and Evans, J. P. (1995) Fluid–rock interactions in faults of crystalline thrust sheets, northwestern Wyoming, U.S.A. Inferences from geochemistry of fault-related rocks. *Journal of Structural Geology* **17**, 533–549.

Handin, J., Hager, R. V., Friedman, M. and Feather, J. N. (1963)

Experimental deformation of sedimentary rocks under confining pressure: pore pressure effects. *American Association of Petroleum Geologists Bulletin* **47**, 717–755.

Haneberg, W. C. (1995) Steady-state groundwater flow across idealized faults. *Water Resources Research* **31**, 1815 1820.

Harding, T. P. and Tuminas, A. C. (1988) Interpretation of foot wall (low side) fault traps sealed by reverse faults and convergent wrench faults. *American Association of Petroleum Geologists Bulletin* **72**, 738–757.

Hubbert, M. K. and Rubey, W. W. (1959) Role of fluid pressure in mechanics of overthrust faulting I. Mechanics of fluid-filled porous solids and its application to overthrust faulting. *Bulletin of the Geological Society of America* **70**, 115–166.

Huntoon, P. W. (1987) The case for regional discharge of ground water from the lower Paleozoic carbonates through the Shay fault zone, Canyonlands, Utah. In *Geology of Cataract Canyon and Vicinity*, ed. J. A. Cambell. Field Symposium Guidebook Four Corners Geological Society **10**, 185–193.

Kastning, E. H. (1977) Faults as positive and negative influences on ground-water flow and conduit enlargement. In *Hydrologic Problems in Karst Regions*, eds R. R. Dilamarter and S. C. Csallany, pp. 193–200. West Kentucky University.

Knipe, R. J. (1992) Faulting processes and fault seal. In *Structural and Tectonic Modelling and its Application to Petroleum Geology*, eds R. M. Larsen, H., Brekke, B. T., Larsen and and E. Talleraas, pp. 325–342. Norak Petroleum Fond Special Publication **1**.

Knott, S. D. (1993) Fault seal analysis in the North Sea. *American Association of Petroleum Geologists Bulletin* **77**, 778–792.

Kranz, R. L., Frankel, A. D., Engelder, T. and Scholz, C. H. (1979) The permeability of whole and jointed Barre granite. *International Journal Rock Mechanics Mineral Science and Geomechanical Abstracts* **16**, 225–234.

Lachmar, T. E. (1994) Application of fracture-flow hydrogeology to acid-mine drainage at the Bunker Hill Mine, Kellogg, Idaho. *Journal of Hydrology* **155**, 125–149.

Levens, R. L., Williams, R. E. and Ralston, D. R. (1994) Hydrogeologic role of geologic structures; Part 1, The paradigm. *Journal of Hydrology* **156**, 227–243.

Lin, C., Pirie, G. and Trimmer, D. A. (1986) Low permeability rocks: laboratory measurements and three-dimensional microstructural analysis. *Journal of Geophysical Research* **91**, 2173–2181.

Lindsay, N. G., Murphy, F. C., Walsh, J. J. and Watterson, J. (1993) Outcrop studies of shale smears on fault surfaces. *Special Publication International Association of Sedimentology* **15**, 113–123.

Lopez, D. L. and Smith, L. (1995) Fluid flow in fault zones: Analysis of the interplay of convective circulation and topographically driven groundwater flow. *Water Resources Research* **31**, 1489–1503.

Lopez, D. L., Smith, L. and Sorey, M. L. (1994) Modeling fluid flow and heat transfer at Basin and Range faults: Preliminary results for Leach Hot Springs, Nevada. *Geothermal Research Council Transactions* **18**, 11–16.

Maclay, R. W. and Groschen, G. E. (1992) Barrier faults control flowpaths within the Edwards Aquifer in the Balcones fault zone, San Antonio area, Texas. *Geological Society of America Abstracts* **24**, 17.

Maclay, R. W. and Small, T. A. (1983) Hydrostratigraphic subdivisions and fault barriers of the Edwards Aquifer, south-central Texas, U.S.A. *Journal of Hydrology* **61**, 127–146.

Martel, S. J. and Peterson, J. E. J. (1991) Interdisciplinary characterization of fracture systems at the US/BK site, Grimsel Laboratory, Switzerland. *International Journal Rock Mechanics Mineral Science and Geomechanical Abstracts* **28**, 295–323.

Martel, S. J. and Pollard, D. D. (1989) Mechanics of slip and fracture along small faults and simple strike-slip fault zones in granitic rock. *Journal of Geophysical Research* **94**, 9417–9428.

Mears, F. (1932) The eight mile Cascade Tunnel, Great Northern Railway Part II. Surveys, construction methods and a comparison of routes. *Transactions of the American Society of Civil Engineers* **96**, 915–1004.

Mitra, G. (1984) Brittle to ductile transition due to large strains along the White Rock thrust, Wind River Mountains, Wyoming. *Journal of Structural Geology* **6**, 51–61.

Morrow, C. A. and Byerlee, J. (1988) Permeability of rock samples from Cajon Pass, California. *Geophysical Research Letters* **15**, 1033 1036.

Morrow, C. A. and Byerlee, J. D. (1992) Permeability of core samples from Cajon Pass scientific drill hole; results from 2100 to 3500 m depth. *Journal of Geophysical Research* **97**, 5145–5151.

Morrow, C. A. and Lockner, D. A. (1994) Permeability differences between surface-derived and deep drillhole core samples. *Geophysical Research Letters* **21**, 2151–2154.

Morrow, C. A., Lockner, D., Hickman, S., Rusanov, M. and Rockel, T. (1994) Effects of lithology and depth on the permeability of core samples from the Kola and KTB drillholes. *Journal of Geophysical Research* **99**, 7274–7623.

Morrow, C. A., Shi, L. Q. and Byerlee, J. D. (1981) Permeability and strength of San Andreas gouge under high pressure. *Geophysical Research Letters* **8**, 325–329.

Morrow, C. A., Shi, L. Q. and Byerlee, J. D. (1984) Permeability of fault gouge under confining pressure and shear stress. *Journal of Geophysical Research* **89**, 3193–3200.

Mozley, P. S. and Goodwin, L. B. (1995) Patterns of cementation along a Cenozoic normal fault: a record of paleoflow orientations. *Geology* **23**, 539–542.

National Research Council (1996) *Rock Fractures and Fluid Flow*. Washington, DC.

Nesbitt, B. E. and Muehlenbachs, K. (1989) Origins and movement of fluid during deformation and metamorphism in the Canadian cordillera. *Science* **245**, 733–736.

Nur, A. and Byerlee, J. D. (1971) An exact effective stress law for elastic deformation of rock with fluids. *Journal of Geophysical Research* **76**, 6414–6419.

Pittman, E. D. (1981) Effects of fault-related granulation on porosity and permeability of quartz sandstones, Simpson Group (Ordovician), Oklahoma. *American Association of Petroleum Geologists Bulletin* **65**, 2381–2387.

Pollard, D. D. and Segall, P. (1987) Theoretical displacements and stresses near fractures in rocks: with applications to faults, joints, veins, dikes, and solution surfaces. In *Fracture Mechanics of Rock*, ed. B. K. Atkinson, pp. 277–349. Academic Press, London.

Randolph, L. and Johnson, B. (1989) Influence of faults of moderate displacement on groundwater flow in the Hickory Sandstone aquifer in central Texas. *Geological Society of America Abstracts* **21**, 242.

Rice, J. R. (1992) Fault stress states, pore pressure distributions, and the weakness of the San Andreas fault. In *Fault Mechanics and Transport Properties of Rock*, eds B. Evans and T.-F. Wong, pp. 475–504. Academic Press, London.

Roberts, S. J. (1995) Episodic expulsion of abnormally pressured fluid along growth faults. *Geological Society of America Abstracts* **27**, A–329.

Robin, P. F. (1973) Note on effective pressure. *Journal of Geophysical Research* **78**, 2435–2437.

Schadt, M. H. (1905) Les resultats scientifiques du percement du tunnel du Simplon. *Bulletin Technique de la Suisse Romande*, 125–178.

Scholz, C. H. (1990) *The Mechanics of Earthquakes and Faulting*. Cambridge University Press, London.

Scholz, C. H. (1994) Permeability of faults. In *The Mechanical Involvement of Fluids in Faulting*, eds S. Hickman, R. L., Bruhn and R. Sibson, pp. 132 137. U.S. Geological Survey Open-File Report 94-228.

Scholz, C. H., Dawers, N. H., Yu, J. Z., Anders, M. H. and Cowie, P. A. (1993) Fault growth and fault scaling laws: preliminary results. *Journal of Geophysical Research* **98**, 21951–21961.

Smith, D. A. (1980) Sealing and nonsealing faults in Louisiana Gulf Coast salt basin. *American Association of Petroleum Geologists Bulletin* **64**, 145–172.

Smith, L., Forster, C. B. and Evans, J. P. (1990) Interaction between fault zones, fluid flow and heat transfer at the basin scale. In *International Association of Hydrologic Sciences Selected Papers in Hydrogeology*, eds S. P. Newman and I. Neretnieks, Vol. 2, pp. 41–67.

Tellam, J. H. (1995) Hydrochemistry of the saline groundwaters of the lower Mersey Basin Permo-Triassic sandstone aquifer, UK. *Journal of Hydrology* **165**, 45–84.

Teufel, L. W. (1987) Permeability changes during shear deformation of fractured rock. *28th U.S. Symposium Rock Mechanics*, pp. 473–480.

Walsh, J. B. (1981) Effect of pore pressure and confining pressure on fracture permeability. *International Journal Rock Mechanics Mineral Science and Geomechanical Abstracts* **18**, 429–435.

Zoback, M. D. and Byerlee, J. D. (1975) Permeability and effective stress. *American Association of Petroleum Geologists Bulletin* **59**, 155–158.